J. Fluid Mech. (1985), *vol.* 155, *pp.* 105–129
Printed in Great Britain

The rheology of concentrated suspensions of spheres in simple shear flow by numerical simulation

By JOHN F. BRADY

Department of Chemical Engineering, Massachusetts Institute of Technology, Cambridge, Massachusetts 02139

AND GEORGES BOSSIS

Laboratoire de Physique de la Matière Condensée, Université de Nice, Parc Valrose, 06034 Nice Cedex

(Received 3 October 1984)

The newly developed simulation method known as Stokesian dynamics is used to investigate the rheological behaviour of concentrated suspensions. Both the detailed microstructure (e.g. pair-distribution function) and the macroscopic properties are determined for a suspension of identical rigid spherical particles in a simple shear flow. The suspended particles interact through both hydrodynamic and non-hydrodynamic forces. For suspensions with purely hydrodynamic forces, the increase in the suspension viscosity with volume fraction ϕ is shown to be caused by particle clustering. The cluster formation results from the lubrication forces, and the simulations of a monolayer of spheres show a scaling law for the cluster size: $l_c \sim [1-(\phi/\phi_m)^{\frac{1}{2}}]^{-1}$, where ϕ_m is the maximum volume fraction that can shear homogeneously. The simulation results suggest that the suspension viscosity becomes infinite at the percolation-like threshold ϕ_m owing to the formation of an infinite cluster. The predicted simulation viscosities are in very good agreement with experiment. A suspension with short-range repulsive interparticle forces is also studied, and is seen to have a non-Newtonian rheology. Normal-stress differences arise owing to the anisotropic local structure created by the interparticle forces. The repulsive forces also reduce particle clustering, and as a result the suspension is shear-thickening.

1. Introduction

Particles suspended in a fluid medium occur throughout nature and industry and exhibit a remarkable variety of rheological properties. Almost every form of non-Newtonian behaviour – shear thinning and thickening, yield stresses, normal-stress differences, etc. – has been observed (Bagnold 1954; Krieger 1972; Jeffrey & Acrivos 1976; Gadala-Maria 1979; Russel 1980; Pätzold 1980; Gadala-Maria & Acrivos 1980). Even a discontinuous viscosity–shear-rate dependence has been reported (Hoffman 1972). The rheological properties of suspensions depend on many factors, of which particle concentration, hydrodynamic, colloidal and Brownian forces, and flow type (simple shear versus extensional flow) are clearly important. The dynamic interaction of these basic factors determines the suspension microstructure, from which the macroscopic rheological properties follow.

Predicting the rheological behaviour of suspensions has been a long-standing

challenge in continuum and statistical mechanics. Theoretical determination of the macroscopic properties originated with the work of Einstein (1906) on the effective viscosity of a dilute suspension of rigid spheres at zero particle Reynolds number. Einstein's celebrated formula for the relative viscosity (the effective viscosity of the suspension divided by the viscosity of the suspending fluid)

$$\eta_r = 1 + \tfrac{5}{2}\phi, \tag{1}$$

where ϕ is the volume fraction of particles, gives the first effect of the particles on the suspension viscosity.

There has been considerable work extending Einstein's formula to second order in volume fraction, thereby bringing in the effects of particle interactions. Corrections to (1) determined by Peterson & Fixman (1963), Batchelor & Green (1972*b*) and others take the form

$$\eta_r = 1 + \tfrac{5}{2}\phi + K\phi^2, \tag{2}$$

where the coefficient K depends on the hydrodynamic interaction between two particles and on the pair-distribution function, i.e. on the suspension microstructure. The analyses of Einstein and Batchelor & Green have been extended in several ways: to non-spherical particles, to include colloidal forces and to include Brownian motion. The review articles by Batchelor (1974), Brenner (1974), Jeffrey & Acrivos (1976) and Russel (1980) summarize much of this work. These theoretical studies of dilute systems have elucidated the fundamental mechanisms operating in suspensions, and provide an important foundation upon which to base further studies. Unfortunately, however, the relative viscosities predicted by (2) agree with experiment only up to volume fractions of the order of 15–20 %.

Extending the dilute-suspension studies to higher concentrations poses two difficult problems: (1) computing the many-body hydrodynamic interactions, and (2) determining the configuration of the microstructure. These problems are so severe that the only rigorous analyses of concentrated suspensions (i.e. above the two-particle limit) that have addressed both of these problems are for spatially periodic models (Adler, Zuzovsky & Brenner 1985; Nunan & Keller 1984). The periodicity allows the many-body interaction problem to be solved exactly on the unit cell, but the assumption of a perfectly regular microstructure is highly restrictive, and is at best only an approximation for a flowing suspension. (A periodic suspension does, however, accurately describe colloidal crystals and may provide a reasonable model for a concentrated suspension undergoing small-amplitude oscillatory motion.) Even within this model, however, the predictions of Adler *et al.* and Nunan & Keller differ as to the asymptotic form of the relative viscosity at close packing.

Nunan & Keller, who compute the relative viscosity only for instantaneous, *static* lattice configurations, find that the viscosity diverges as

$$\eta_r \sim \frac{1}{1-(\phi/\phi_m)^{\frac{1}{3}}} \tag{3}$$

as the volume fraction approaches the maximum ϕ_m for that particular lattice. This singular behaviour is the same as that found by Frankel & Acrivos (1967) based on a lubrication-type argument. The fundamental assumption underlying their analysis is that at close packing the relative velocity between two particles remains finite as the particles are pushed together (or pulled apart) by the shear flow. Lubrication theory requires an infinite force to push surfaces together at finite velocity, and hence the singularity in (3). Frankel & Acrivos' model is also static, containing no information on the dynamics of the microstructure, and does not offer any explanation

as to the origin of this infinite force. In the spatially periodic case, the relative velocity must, of necessity, be finite at touching.

At the same time, Adler *et al.*, who treat the same spatially periodic case as Nunan & Keller, but consider the *dynamics* of the suspension by averaging in time over the many different lattices sampled by the steadily sheared suspension, show that the singularity (3) disappears on averaging. This very interesting result is explained as follows. Although the lubrication forces are singular as ξ^{-1}, where ξ is the separation between the particle surfaces, the 'area' of closest contact is $O(\xi)$, and the resulting viscosity is thus $O(1)$. Said differently, since the periodicity of the flow requires particles to translate with a *constant* relative velocity, the time spent at closest contact is only $O(\xi)$, and thus the contribution to the viscosity from this lubrication region is $O(1)$. The essentially static analyses of Frankel & Acrivos and Nunan & Keller implicitly assume the time spent at close contact is $O(1)$. Thus the supposed singular behaviour of the relative viscosity, which has been widely accepted by both experimentalists and theoreticians, depends fundamentally on the dynamics of the suspension microstructure, is absent for spatially periodic suspensions, and remains an unresolved question for non-periodic microstructures.

Recently, Beenakker (1984) has developed a theory for suspension viscosity which includes formally the complete many-body hydrodynamic interactions. These interactions are determined in the form of infinite series of multiple reflections, and by a judicious ordering of the sphere–sphere reflections certain types of interactions may be summed. While formally correct, all interactions have not been summed and thus not included, and the microstructure is not determined; a Percus–Yevich hard-sphere distribution is assumed. A further discussion of this theory and other approaches is given in §3.

There have of course been many other approaches, theories, correlations and ideas put forth to explain and predict the rheological behaviour of suspensions. Our purpose here is not to review the literature but rather to briefly summarize our present theoretical understanding and to point out those approaches we shall refer to later.

In an effort to understand the behaviour of concentrated suspensions, we have recently developed a general method for numerically simulating the dynamics of many interacting particles in Stokes flow (Bossis & Brady 1984). This method, which we have named Stokesian dynamics, uses a molecular-dynamics-like approach to follow the time evolution of the positions of particles in suspension. Thus many-body effects are taken into account and the suspension microstructure evolves dynamically. The particles interact through both hydrodynamic and non-hydrodynamic forces, the latter of which may be almost any type of Brownian, colloidal, interparticle or external force. The key feature of the method is, however, the hydrodynamic interactions. The method is quite versatile, and has already offered new insights into suspension structure, such as an anisotropic local structure and, under certain circumstances, a transition to a highly ordered state at high concentrations, both of which are shear-induced. In this paper we report on the macroscopic rheological properties that can be determined from Stokesian-dynamics simulations.

In §2 we shall briefly summarize the salient features of the Stokesian-dynamics method; the details can be found in our earlier paper. We shall then show how to compute the rheological properties of suspensions by numerical simulation. With Stokesian dynamics the complete instantaneous and time-averaged bulk stress (Batchelor 1970) can be determined, from which both the effective viscosity and normal-stress differences can be computed. Specific calculations are carried out for a monolayer of identical rigid non-Brownian spheres in a simple shear flow. In a

monolayer (cf. figure 1) all particles lie in the same plane, the plane of shear. While an idealized model suspension, a monolayer is a realizable suspension flow, and experiments have been performed on such systems (Belzons *et al.* 1981; Bouillot *et al.* 1982). A monolayer provides a convenient numerical setting because it minimizes the computation costs while preserving the essential physics in the plane of shear, i.e. it is expected that the pair-distribution function in the plane of shear will not differ significantly from that in a fully three-dimensional suspension.

In §3 we present the effective viscosity and normal-stress differences for two types of suspensions. In the first, particles interact through purely hydrodynamic forces. In this case the effective viscosity can be expressed solely as a function of the volume fraction. The normal-stress differences are statistically zero because the distribution of particles is symmetric in the plane of shear, a result, no doubt, of the reversibility of Stokes flow. It will be shown that the increase in the suspension viscosity with increasing density is due to two effects: (1) the change in microstructure, i.e. the distribution of particles, and (2) the increase in the relative velocity of two particles. It is the latter effect that gives rise to the rapid increase in the viscosity with concentration. We show that this increase in relative velocity can be interpreted in terms of an 'effective' shear rate due to particle clustering. Our numerical results suggest that the cluster size scales with the lubrication forces, as given by a formula similar to (3), indicating that the suspension viscosity becomes infinite owing to the formation of an infinite cluster. In this section we also compare our numerically determined suspension viscosities with experiment and with the recent theoretical calculations of Beenakker (1984).

The second type of suspension investigated is one where, in addition to the hydrodynamic shear forces, the particles interact through repulsive DLVO-type colloidal forces. The viscosity now depends on three parameters: the volume fraction, the shear rate, i.e. the ratio of hydrodynamic to colloidal forces, and a parameter that characterizes the range (as opposed to amplitude) of the colloidal forces, which in our case is a non-dimensional Debye length. The non-hydrodynamic interparticle forces affect the bulk stress in two ways: (1) there is a direct 'elastic' contribution to the stress (cf. (10) below), and (2) the interparticle forces influence the particle trajectories, changing the microstructure. This suspension with short-range repulsive forces is shear-thickening due primarily to the change in microstructure with shear rate. Normal-stress differences are also present because the microstructure is locally anisotropic.

2. Simulation method

The details of the Stokesian-dynamics method can be found in Bossis & Brady (1984); here we only sketch the main points. In the absence of Brownian motion and at low particle Reynolds number, the equations of motion for N particles suspended in a Newtonian solvent undergoing a bulk linear shear flow may be written as

$$-\boldsymbol{R}\cdot\boldsymbol{U}^{*}+\boldsymbol{\Phi}:\boldsymbol{E}+F_{\mathrm{p}}=0. \tag{4}$$

In (4) $\boldsymbol{U}^{*}$ is a vector of dimension $6N$ containing the translational–rotational velocities of the N particles relative to the bulk fluid's translational–rotational velocity evaluated at the particles' centres $\boldsymbol{U}^{0}$. The $6N\times 6N$ grand resistance matrix $\boldsymbol{R}$ depends on the instantaneous configuration of all N particles and gives the force–torque exerted by the fluid on the particles due to their motion relative to the fluid. The $6N\times 3\times 3$ matrix $\boldsymbol{\Phi}$ is also configuration-dependent and gives the

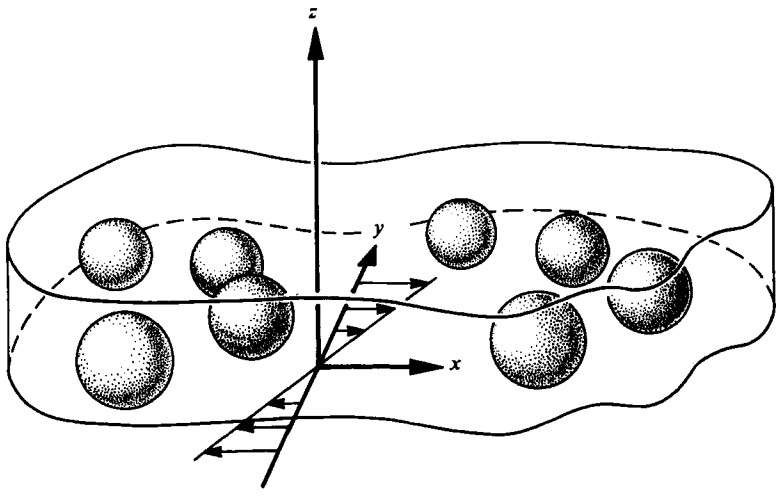

FIGURE 1. Schematic diagram of a sheared monolayer. All spheres are of the same radius and lie in the plane of shear.

force–torque on the particles due to the bulk shear flow. For simple shear in the (x, y)-plane (cf. figure 1) the bulk rate-of-strain tensor $\boldsymbol{E}$ is given by

$$\boldsymbol{E} = \frac{\dot{\gamma}}{2}\begin{bmatrix} 0 & 1 & 0 \\ 1 & 0 & 0 \\ 0 & 0 & 0 \end{bmatrix}, \tag{5}$$

where $\dot{\gamma}$ is the shear rate, and the bulk vorticity $\boldsymbol{\Omega}$ is

$$\boldsymbol{\Omega} = -\tfrac{1}{2}\dot{\gamma}\,(0, 0, 1). \tag{6}$$

How the bulk quantities $\boldsymbol{E}$ and $\boldsymbol{\Omega}$ relate to the mechanism causing the shear is discussed below. $\boldsymbol{F}_{\mathrm{p}}$ stands for any non-hydrodynamic forces acting on the particles, such as interparticle colloidal forces or an external force such as gravity.

In linear shear flow where $\dot{\gamma}^{-1}$ sets the timescale, the condition for the neglect of particle inertia is that the particle Reynolds number $Re = \rho\dot{\gamma}a^2/\eta$ be much less than unity. ρ is the suspending fluid's density and η its viscosity. In order to neglect Brownian motion, the particle Péclet number $Pe = 6\pi\eta a^3/kT$ must be large. Here k is Boltzmann's constant, T is the absolute temperature and we have used the Stokes–Einstein relation for the particle diffusivity $D = kT/6\pi\eta a$, which overestimates the diffusivity in a suspension. There are many situations in which both conditions are satisfied; e.g. spherical particles in excess of 5 μm in diameter in water at room temperature have Péclet numbers $O(100)$ for shear rates $O(1\ \mathrm{s}^{-1})$, while the same particles have Reynolds numbers $O(10^{-5})$. In the simulations discussed here these conditions are assumed to be satisfied.

While the evolution equation (4) is exact, approximations are needed for the grand and shear resistance matrices because the many-body hydrodynamic theories that have been advanced (Beenakker 1984; Beenakker & Mazur 1983; Mazur & van Saarloos 1982) are not yet in a form suitable for dynamic simulations. Thus the resistance matrices $\boldsymbol{R}$ and $\boldsymbol{\Phi}$ are constructed by a pairwise superposition of the exact two-sphere results. Although it is desired to obtain the velocities $\boldsymbol{U}^*$, which requires

inverting the resistance matrix to obtain the so-called mobility matrix $\boldsymbol{R}^{-1}$, it is necessary to add interactions pairwise in $\boldsymbol{R}$ rather than in $\boldsymbol{R}^{-1}$. Pairwise additivity in $\boldsymbol{R}$ corresponds to a superposition of forces, while a pairwise additivity in $\boldsymbol{R}^{-1}$ corresponds to a superposition of velocities. Pairwise interactions in $\boldsymbol{R}$ maintain the hydrodynamic lubrication forces that prevent particles from overlapping. In the mobility matrix the lubrication forces are lost, and particles freely overlap unless there are strong repulsive interparticle forces. The exact two-sphere results for $\boldsymbol{R}$ and $\boldsymbol{\Phi}$ are given in Arp & Mason (1977), Jeffrey & Onishi (1984), Jeffrey (1984 personal communication) and Kim & Mifflin (1985).

Pairwise additivity is of course an approximation, but one that has proved useful in molecular dynamics and that we hope to demonstrate is also useful, if not accurate, in Stokesian dynamics. In dense suspensions the lubrication forces are the most important, and these are modelled correctly by the superposition of forces. Three-body and higher-order effects found from far-field expansions will fade in comparison with the lubrication forces as the separation distances become small. When three-body effects become important in concentrated systems, four-body and higher-order effects are also of the same order and would need to be included. In dilute suspensions most interactions are pairwise, and again pairwise additivity should be accurate. Thus pairwise additivity in the resistance matrix seems to contain the essential physics. It should be noted, however, that inverting the resistance matrix to find the particle velocities involves more than what a strict pairwise additivity normally implies, and many-body interactions are actually taken into account.

The many-body interactions included can be understood in the following way. Each particle in suspension acts as a series of multipoles whose strengths are unknown *a priori* and depend on the relative positions of all particles, as well as the bulk shear flow. The strengths of these multipoles are ultimately determined by the condition that the net force–torque on each particle is, in the absence of non-hydrodynamic forces, zero. In the resistance formulation the strengths of the multipoles on all particles are determined simultaneously by inverting $\boldsymbol{R}$ such that the net force–torque on all particles in the N-body system is zero. The resulting particle velocities are such that this N-body force–torque requirement is satisfied. In the mobility formulation the net force–torque for each particle in a *pair* is zero, and the strengths of the multipoles and the velocities are determined from this two-body requirement only. The sum over all pairs then gives the resultant motion.

The superposition of forces can also be viewed simply as one way in which to approximate the complex, configuration-dependent, matrix $\boldsymbol{R}$. The remainder of the calculations proceed just as if we knew the exact N-body matrix. The method works because the approximation captures the correct physics at both large and small separations. The same cannot be said for the superposition of velocities in the mobility matrix.

To model a suspension of 'infinite' extent periodic boundary conditions are used. For the simple shear flow represented by (5) and (6) the periodic conditions in the x- and z-directions are straightforward, but periodicity in y requires a translation in x by an amount $H\dot{\gamma}t$ in order to preserve the bulk linear shear flow (Evans 1979; Bossis & Brady 1984). Here H is the periodic box height in the y-direction and t is time. By periodic boundary conditions the suspension is represented as a spatially periodic array of identical cells, and it can be proved (Adler *et al.* 1985) that the bulk rate of strain $\boldsymbol{E}$ and vorticity $\boldsymbol{\Omega}$ are indeed well-defined macroscopic constants. Thus simple shear with periodic boundary conditions is well-posed and is intended to model the behaviour of a suspension far removed from the boundaries creating the flow. To

include boundary effects the formulation (4) cannot be used, because a bulk linear shear flow does not necessarily exist. As in all dynamic simulations the periodic cell must be sufficiently large so as not to affect the results. One measure that this requirement is satisfied is that the pair-distribution function approaches the bulk density, i.e. all structure is lost, before the edge of the periodic cell is reached.

In using periodic boundary conditions a particle interacts only with its nearest neighbours in the periodic cell; interactions with particles outside the cell are neglected. By using an argument based on the work of O'Brien (1979) it can be shown that, although the hydrodynamic interactions are long-ranged, falling off as r^{-2} for force-free particles, particles outside the periodic cell *in total* contribute zero to the translational–rotational velocity of the particle at the centre of its periodic cell with an error $O(R^{-2})$, where R is a characteristic dimension of the cell. As the size of the periodic cell increases, the effect of the surrounding particles can be made arbitrarily small. This same argument can be used when the non-hydrodynamic forces are only between particles.

Although this can be proven rigorously, there is also a simple physical explanation. As far as the particle at the centre of the periodic cell is concerned, particles outside this volume appear, not as discrete particles, but as a continuous distribution of force dipoles whose dipole strength depends on the bulk rate of strain $\boldsymbol{E}$. This uniform distribution of dipoles gives zero contribution to the translational–rotational velocity of the central particle. The principal errors come in representing the discrete distribution as a continuous one and in assuming that the dipole strength of the continuous distribution is just its bulk-average value. The latter error is at most $O(R^{-2})$, and the former depends on precisely how fast the discrete distribution approaches the continuous one. Our simulations indicate that this approach is sufficiently fast for the above error estimate to be valid. Note, however, that the particles outside the cell *do* contribute to the central particle's stresslet and hence to the bulk stress, as we now discuss.

The bulk rheological properties of the suspension are determined from the average stress tensor (Batchelor 1970). In the presence of interparticle forces there are two contributions to the bulk stress: the mechanical or contact stress transmitted by the fluid, and the 'elastic' stresses due to the interparticle forces themselves. The general form for both types of stresses can be found in Batchelor (1977). The average or bulk stress can be written as

$$\langle \boldsymbol{\sigma} \rangle = \text{I.T.} + 2\eta \boldsymbol{E} + \frac{N}{V} \{ \langle \boldsymbol{S}^{\text{H}} \rangle + \langle \boldsymbol{S}^{\text{P}} \rangle \}. \tag{7}$$

Here $\langle \boldsymbol{\sigma} \rangle$ is the average stress, I.T. stands for an isotropic term of no interest, N is the number of particles in the averaging volume V, and $\langle \boldsymbol{S}^{\text{H}} \rangle$ and $\langle \boldsymbol{S}^{\text{P}} \rangle$ are the particle contributions to the contact and elastic stresses respectively.

The contact or hydrodynamic average particle stress $\langle \boldsymbol{S}^{\text{H}} \rangle$ is given by

$$(1-\phi) \langle \boldsymbol{S}^{\text{H}} \rangle = \frac{1}{N} \sum_{\alpha=1}^{N} \boldsymbol{S}^{\alpha} = \frac{1}{N} \sum_{\alpha=1}^{N} \{ \boldsymbol{G}^{\alpha} \cdot \boldsymbol{U}^{*} - \boldsymbol{M}^{\alpha} : \boldsymbol{E} \}. \tag{8}$$

The summation is over all particles in the averaging volume, $\boldsymbol{S}^{\alpha}$ is the stresslet of particle α, which from linearity can be expressed in terms of all the particles' velocities and the bulk rate of strain through $\boldsymbol{G}^{\alpha}$ and $\boldsymbol{M}^{\alpha}$. $\boldsymbol{G}^{\alpha}$ and $\boldsymbol{M}^{\alpha}$ are configuration-dependent and given explicitly in Jeffrey (1984 personal communication) and Kim & Mifflin (1985). (In these works $\boldsymbol{G}^{\alpha}$ is separated into translational and rotational parts.) The reciprocal theorem relates many of the elements of $\boldsymbol{G}^{\alpha}$ to $\boldsymbol{\Phi}$. Again $\boldsymbol{G}^{\alpha}$ and $\boldsymbol{M}^{\alpha}$ are constructed by a pairwise superposition of the exact two-sphere results.

The factor $1-\phi$, where ϕ is the volume fraction, represents the effect of all the particles outside the averaging volume on the particle stress. This is the effect referred to above in the discussion of O'Brien's work and periodic boundary conditions. In the dilute limit when the spherical particles are isolated, $\boldsymbol{S}^{\alpha} = \frac{20}{3}\pi\eta a^3 \boldsymbol{E}$, and $\langle \boldsymbol{S}^{\mathrm{H}} \rangle$ from (8) gives a bulk stress in (7)

$$\frac{N}{V}\langle \boldsymbol{S}^{\mathrm{H}} \rangle = \frac{5\phi}{1-\phi}\boldsymbol{E} \approx 5\phi \boldsymbol{E}, \tag{9}$$

which is just Einstein's result (1). Keeping the next term in expanding the denominator of (9) gives the $5\phi^2\boldsymbol{E}$ 'kinematical' correction of Batchelor & Green (1972*b*) (cf. their equation (4.2) and the discussion that follows). The expression (8) for the particle stress is essentially equation (3.15) of O'Brien (or his later (4.3)), which he derived for the effective thermal conductivity, applied to the bulk stress. The derivation follows exactly the procedure used by O'Brien.

The elastic contribution to the particle stress $\langle \boldsymbol{S}^{\mathrm{P}} \rangle$ can be written as (Batchelor 1977)

$$\langle \boldsymbol{S}^{\mathrm{P}} \rangle = -\frac{1}{N}\sum_{\alpha=2}^{N}\sum_{\beta<\alpha} \boldsymbol{r}^{\alpha\beta}\boldsymbol{F}^{\alpha\beta}, \tag{10}$$

where $\boldsymbol{r}^{\alpha\beta}$ is the centre–centre separation of particles α and β, and $\boldsymbol{F}^{\alpha\beta}$ is their pairwise interparticle force. The addition of the pairwise forces $\boldsymbol{F}^{\alpha\beta}$ gives the non-hydrodynamic force $\boldsymbol{F}_{\mathrm{p}}$ in the evolution equation (4).

Equation (7), (8) and (10) complete the definition of the bulk stress. The only assumptions made, in addition to the restrictions on the Péclet and Reynolds numbers, are that the suspension is statistically homogeneous and that there are no body couples so that the bulk stress is symmetric. Body couples can readily be included if one wishes to investigate antisymmetric stresses of the type found in magnetic fluids. Even though the interparticle forces investigated here are of electrostatic origin, no account is taken of the stresses due to the deformation of the double layers themselves, the so-called primary electroviscous effect (Russel 1978). The double layers considered here are very thin and this contribution is small.

Since $\boldsymbol{G}^{\alpha}$, $\boldsymbol{M}^{\alpha}$ and $\boldsymbol{F}^{\alpha\beta}$ are configuration-dependent, (7) determines the *instantaneous* bulk stress. The bulk rate of strain $\boldsymbol{E}$ and vorticity $\boldsymbol{\Omega}$, while constant in space, can be arbitrary functions of time, and thus (7) allows the investigation of dynamic rheological properties as might be measured in an oscillatory shear experiment. The simulations to be discussed here are all steady, and (7) is averaged in time to give the time-average bulk stress.

The above considerations for Stokesian dynamics and the definition of the bulk stress are true for any homogeneous suspension. Before closing this section, we apply these general results to our monolayer suspensions. Since all particles are constrained to lie in the (x, y)-plane as illustrated in figure 1, the number of degrees of freedom for each sphere is reduced from 6 to 3, with an 8-fold saving in computation time. The averaging volume V is now the volume of the monolayer $V = 2aA$, where a is the sphere radius and A is the area of the periodic cell. Rather than a volume fraction, we now have an areal fraction $\phi_A = \pi a^2 N/A$, where N is now the number of particles in the area A.

Using a monolayer suspension has several noticeable effects on the bulk stress. The stress components $\langle \sigma_{zx} \rangle$ and $\langle \sigma_{zy} \rangle$ are zero because of the two-dimensional nature of the motion. The coefficient for the Einstein limit of non-interacting particles is $\frac{5}{3}\phi_A$ rather than $\frac{5}{2}\phi$, i.e. (9) simply gives $\frac{10}{3}\phi_A \boldsymbol{E}$. This can also be viewed as $\phi_A = \frac{2}{3}\phi$. Also

the contribution $\phi\langle \boldsymbol{S}^{\mathrm{H}} \rangle$ coming from the particles outside the averaging volume is not present. The reason for this can be explained in two ways: (1) the volume fraction in a three-dimensional sense of the monolayer is zero, and (2) defining the bulk stress as an areal average rather than a volume average will show that, since all particles lie in the same plane, adding contributions from far particles is now a convergent process. The contribution from far particles to the stresslet of the central particle α decays as r^{-3}, but the number of particles only grows as r^2, so the summation is convergent.

The effective viscosity of the suspension is defined as the ratio of the (x, y)-component of the average stress to the shear rate:

$$\eta_{\mathrm{r}} \equiv \frac{\langle \sigma_{xy} \rangle}{2\eta E_{xy}} = 1 + \frac{1}{\eta\dot{\gamma}} \frac{N}{V} \{\langle S^{\mathrm{H}}_{xy} \rangle + \langle S^{\mathrm{P}}_{xy} \rangle\}. \tag{11}$$

The normal-stress differences define the primary and secondary normal-stress coefficients Ψ_1 and Ψ_2 common in the polymer-rheology literature:

$$\langle \sigma_{xx} \rangle - \langle \sigma_{yy} \rangle \equiv -\dot{\gamma}^2 \Psi_1, \tag{12}$$

$$\langle \sigma_{yy} \rangle - \langle \sigma_{zz} \rangle \equiv -\dot{\gamma}^2 \Psi_2. \tag{13}$$

Care must be exercised in using the expression $\boldsymbol{G}^{\alpha} \cdot \boldsymbol{U}^* - \boldsymbol{M}^{\alpha} : \boldsymbol{E}$ for the particle stresslet in (8), because each of the two terms is singular as two particles approach one another, but their difference is not. That is, when two particles touch, their stresslets remain finite. In order to avoid possible numerical round-off error $\langle \boldsymbol{S}^{\mathrm{H}} \rangle$ can be rearranged and rewritten as a sum over pairs of particles as in (10). Not only is this formulation more accurate numerically, it also isolates contributions to the effective viscosity that come from the relative velocities of two particles and from the shear rate. We shall see below that this rearrangement offers considerable insight into the mechanisms causing the suspension viscosity. Making use of the known, exact, two-sphere expressions for $\boldsymbol{G}^{\alpha}$ and $\boldsymbol{M}^{\alpha}$ (Jeffrey 1984 personal communication; Kim & Mifflin 1985), and after considerable tedious algebra, the effective viscosity (11) can be written as

$$\begin{aligned}
\eta_{\mathrm{r}} = 1 &+ \tfrac{5}{3}\phi_A - 2\phi_A \frac{1}{N} \sum_{\alpha=2}^{N} \sum_{\beta<\alpha} \Bigg\{ (\hat{X}^G_{11} - \hat{X}^G_{12}) \frac{\sin 2\theta_{\alpha\beta}}{2} \Delta U_r^{\alpha\beta} \\
&+ (\hat{Y}^G_{11} - \hat{Y}^G_{12}) \cos 2\theta_{\alpha\beta} \, \Delta U_t^{\alpha\beta} + 2(\hat{Y}^H_{11} + \hat{Y}^H_{12}) \cos 2\theta_{\alpha\beta} \, (\Omega_z^{\alpha} + \Omega_z^{\beta}) \\
&+ \Bigg[\hat{r}^{\alpha\beta} (\hat{X}^G_{11} - \hat{X}^G_{12}) \frac{(\sin 2\theta_{\alpha\beta})^2}{4} - \hat{r}^{\alpha\beta} (\hat{Y}^G_{11} - \hat{Y}^G_{12}) \cos 2\theta_{\alpha\beta} \sin^2 \theta_{\alpha\beta} \\
&+ 2(\hat{Y}^H_{11} + \hat{Y}^H_{12}) \cos 2\theta_{\alpha\beta} \\
&- \tfrac{5}{3}(3\hat{X}^M_{1112} + \hat{Z}^M_{1112} - 4\hat{Y}^M_{1112}) \frac{(\sin 2\theta_{\alpha\beta})^2}{4} - \tfrac{5}{3} \hat{Y}^{M*}_{1112} \Bigg] \Bigg\} \\
&- \frac{3\phi_A}{\dot{\gamma}^*} \frac{1}{N} \sum_{\alpha=2}^{N} \sum_{\beta<\alpha} \hat{r}^{\alpha\beta} \hat{F}_r^{\alpha\beta} \frac{\sin 2\theta_{\alpha\beta}}{2}.
\end{aligned} \tag{14}$$

In (14) $\theta_{\alpha\beta}$ is the angle between particles α and β measured relative to the x-axis with particle α at the origin (cf. inset in figure 4). $\Delta U_r^{\alpha\beta}$ is the actual (i.e. the contribution from the shear flow has not been subtracted off as in $\boldsymbol{U}^*$) relative radial (along the line of centres) velocity of spheres α and β made non-dimensional with $a\dot{\gamma}$. $\Delta U_t^{\alpha\beta}$ is their actual tangential relative velocity, and Ω_z^{α} and Ω_z^{β} are the actual

rotational velocities, which only have a z-component. The functions $\hat{X}^G_{11}$, $\hat{X}^G_{12}$ etc. are non-dimensional functions of the scalar centre–centre separation $\hat{r}^{\alpha\beta}$, which has been non-dimensionalized by the sphere radius a. The notation and the non-dimensionalizations are those of Jeffrey (1984 personal communication) and Kim & Mifflin (1985). The superscript * on $\hat{Y}^M_{1112}$ is to indicate that the self-stresslet (i.e. for isolated particles) has been removed, giving rise to the $\frac{5}{3}\phi_A$ term. In the interparticle-force term $\hat{F}^{\alpha\beta}_r$ is the radial force exerted by sphere β on α (which is equal and opposite to $\hat{F}^{\beta\alpha}_r$) non-dimensionalized by its amplitude $|F_0|$. $\dot{\gamma}^* = 6\pi\eta a^2\dot{\gamma}/|F_0|$ is the non-dimensional shear rate. If there were only two particles in suspension, the relative velocities could be expressed in terms of the rate of strain by the mobilities, and (14) would reduce to the two-particle stresslet of Batchelor & Green (1972*b*).

In (14) we can identify five separate contributions to the effective viscosity: (1) the radial, (2) the tangential and (3) the rotational velocity terms, (4) the term in square brackets, which comes directly from the bulk shear flow, and (5) the interparticle force term. The angular dependence is symmetric about $\theta_{\alpha\beta} = \frac{1}{2}\pi$, indicating that as much energy is dissipated bringing two particles together ($\theta_{\alpha\beta} > \frac{1}{2}\pi$) as in pulling them apart ($\theta_{\alpha\beta} < \frac{1}{2}\pi$). All the microstructural information on the spatial and temporal distribution of particles found from solving the evolution equation (4) is present as the sum over particle pairs. As $\dot{\gamma}^* \to \infty$ the shear forces dominate the interparticle forces, both in (14) and in (4), and the viscosity depends only on the microstructure, which in turn depends only on the volume fraction.

In this formulation the contributions to the stress from particles α and β are no longer singular. Although the coefficient $\hat{X}^G_{11} - \hat{X}^G_{12}$ of the radial-velocity term behaves as ξ^{-1} as $\xi = \hat{r}^{\alpha\beta} - 2 \to 0$, the relative radial velocity $\Delta U^{\alpha\beta}_r$ decreases proportionally with ξ. For two isolated spheres Batchelor & Green (1972*a*) found that $\Delta U^{\mathrm{B}}_r \sim -4.077\xi$ as $\xi \to 0$, and for all the densities we have simulated we find the same dependence on ξ, but with a coefficient that is volume-fraction-dependent. It is this coefficient that has a scaling law of the form given by (3), as we discuss below. The Y-coefficients in the tangential and rotational velocity terms are logarithmically singular as $\xi \to 0$, but their combination in line 2 of (14) is not. Similarly, the bracketed term in (14) coming from the shear flow is $O(1)$. Depending on the nature of the interparticle force $\hat{F}^{\alpha\beta}_r$, this term may appear to be singular as $\xi \to 0$, but when combined with the radial-velocity term and account taken of the resulting microstructure it results in a finite particle stress.

Analogous expressions can be written for the normal-stress coefficients Ψ_1 and Ψ_2, but we shall not present the rather lengthy formulae here, as they contain little new information. As in (14), the two-particle stresslets are non-singular as $\xi \to 0$. One important difference, however, is that Ψ_1 and Ψ_2 are antisymmetric about $\theta_{\alpha\beta} = \frac{1}{2}\pi$. This implies, as first noticed by Batchelor & Green (1972*b*), that normal-stress differences arise only when the distribution of particles is not symmetric in the plane of shear. Not surprisingly, in our simulations non-symmetric distributions, and hence normal-stress differences, occur only in the presence of interparticle forces.

3. Results

The rheological properties were determined for two types of suspensions: with and without interparticle forces. In both systems 25 particles were used, as this number yields affordable computation times and still contains enough particles to include all second-nearest neighbours. (For hexagonal close packing in a plane a central particle has 6 nearest and 12 next-nearest neighbours.) In our earlier work we also showed

that the pair-distribution function determined with 25 particles is in statistical agreement with that found with 100 particles. The simulations all started with the particles located at random in the periodic cell, and were integrated in time until a stationary state was reached. The stationarity was determined by monitoring the average of the square of the x- and y-components of the particle velocities relative to the bulk shear flow. With a normal dimensionless time step of 4×10^{-3}, stationarity was reached in approximately 5000 time steps, and the calculations were generally carried out to a total of 20000 time steps. The pair-distribution functions $g(r)$ reported below and the bulk stress were averaged in time over the last 15000 time steps. To determine the statistical errors, sample simulations under the same conditions of areal fraction and interparticle force were run starting from different initial conditions and for a total of 60000 time steps. We report here simulation results for areal fractions up to 0.5. More-dense systems begin to become expensive, as the time step must be reduced to accurately follow the particle trajectories. All calculations were performed in double precision on an IBM 3033 and/or a Cray 1.

3.1. *Pure hydrodynamics*

In the absence of interparticle forces the bulk stress is a function only of the volume fraction; the shear rate $\dot{\gamma}$ simply sets the timescale. With our simulations we naturally find that the suspension viscosity increases with increasing volume fraction, but, in order to understand the mechanisms that cause this increase and to make comprehensible the wealth of statistical information available to us, we shall discuss the effective viscosity primarily in terms of two bodies. Comparison will also be made with the dilute theories and with the work of Beenakker (1984).

An examination of (14) will reveal that there are two basic factors that determine the viscosity in dense suspensions: (1) the distribution of particle pairs, i.e. the microstructure, and (2) the fact that the relative velocities of two particles are not the same as they would be if there were only two particles in suspension. In figure 2 we compare the relative viscosities determined by simulation (solid circles) with the viscosities found from the two-sphere $O(\phi^2)$ analysis of Batchelor & Green (1972*b*) under two conditions. In the first (open circles), the coefficient K in (2) is calculated assuming that the distribution of particles outside the excluded volume $r < 2$ is uniform and equal to the bulk density. In the second (open squares), we use the same two-sphere analysis, but with the actual distribution of particles found in our simulations.

We first note that the simulation viscosities are uniformly larger than the two-sphere ones, although at low densities, $\phi_A = 0.1$, all three calculations agree as one should expect. What is interesting, however, is that the two-sphere viscosity with the correct microstructure is lower than that found by assuming a uniform density. This behaviour can be understood with the help of figures 3–5.

In figure 3 we present the cumulative contribution to the two-sphere viscosity as a function of separation r of the two spheres at an areal fraction of 0.4. With the uniform density there is a slow monotonic increase in the viscosity as the area, and hence the number of particles, increases. The viscosity reaches a limit because the stresslet eventually decays as r^{-3}. With microstructure the two-sphere viscosity rises rapidly, followed by a very slow monotonic increase, eventually reaching a lower value than without structure. Examination of the pair-distribution function will explain this behaviour.

The pair-distribution function $g(r, \theta)$ is shown in figures 4 and 5, displaying separately its angular, $g_{\Delta r}(\theta)$, and radial, $\langle g(r) \rangle_\theta$, dependence. Shown in figure 4 for two

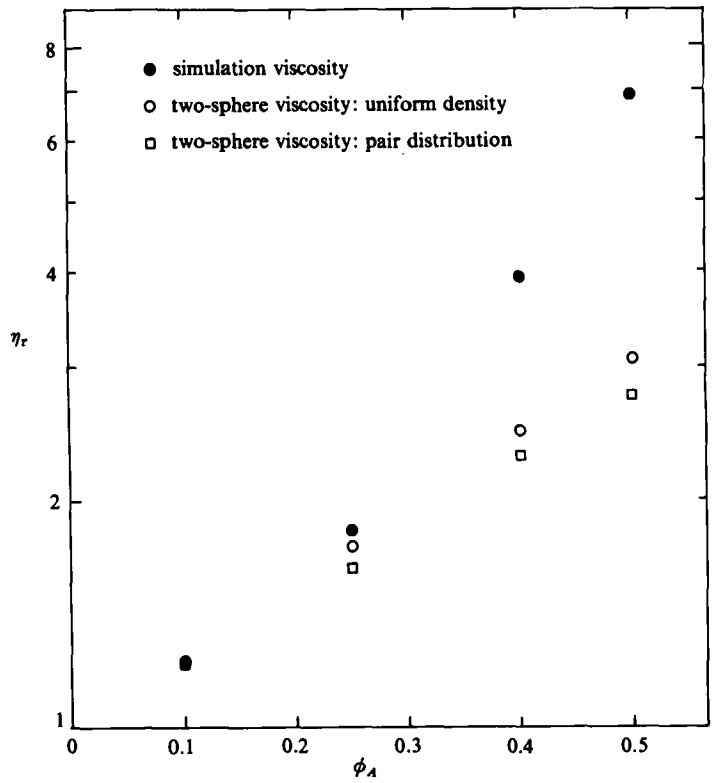

FIGURE 2. Comparison of the suspension viscosity η_r obtained by simulation (●) with the two-sphere $O(\phi^2)$ viscosity calculated from the analysis of Batchelor & Green (1972*b*) as a function of areal fraction ϕ_A: ○ assumes a uniform density of particles, and □ uses the pair-distribution function found by simulation.

areal fractions, $\phi_A = 0.1$ and 0.4, is the angular dependence of the pair-distribution function in the Δr range $2 < r < 2.05$, which includes the first-nearest-neighbour peak. The angular structure is relatively weak, but yet statistically significant, and is symmetric about $\theta = \frac{1}{2}\pi$, i.e. there are no normal-stress differences. At low densities, where most interactions are between only two particles, the angular distribution has its maxima at $\theta = 0$ and π, and passes through a minimum at $\theta = \frac{1}{2}\pi$. This is consistent with what is known for two isolated spheres: a two-sphere dumbbell spends more time aligned with the shear ($\theta = 0$ and π) than at right-angles to it ($\theta = \frac{1}{2}\pi$), and thus the probability density for pairs should reflect this. Some recent experiments of Husband & Gadala-Maria (1984), where the angular dependence in the plane of shear of the pair-distribution function in dilute three-dimensional suspensions ($\phi < 0.05$) was measured, are in good agreement with our results for $\phi_A = 0.1$. At higher densities the angular dependence is reversed, with the maximum occurring at $\theta = \frac{1}{2}\pi$. Here, as the dumbbell of two spheres tries to rotate in the shear flow, its movement is hindered by the other particles, so it actually spends more time perpendicular to the flow direction than aligned with it. The weak angular structure has little effect, however, on the suspension viscosity.

The radial dependence of the pair-distribution function $\langle g(r)\rangle_\theta$ at $\phi_A = 0.4$ shown in figure 5 is a simple θ-average of $g(r, \theta)$. $\langle g(r)\rangle_\theta$ is strongly peaked at the minimum separation distance $r = 2$ (see inset), drops rapidly to below the bulk density level of 1, and then peaks again at the second-nearest-neighbour position before approaching

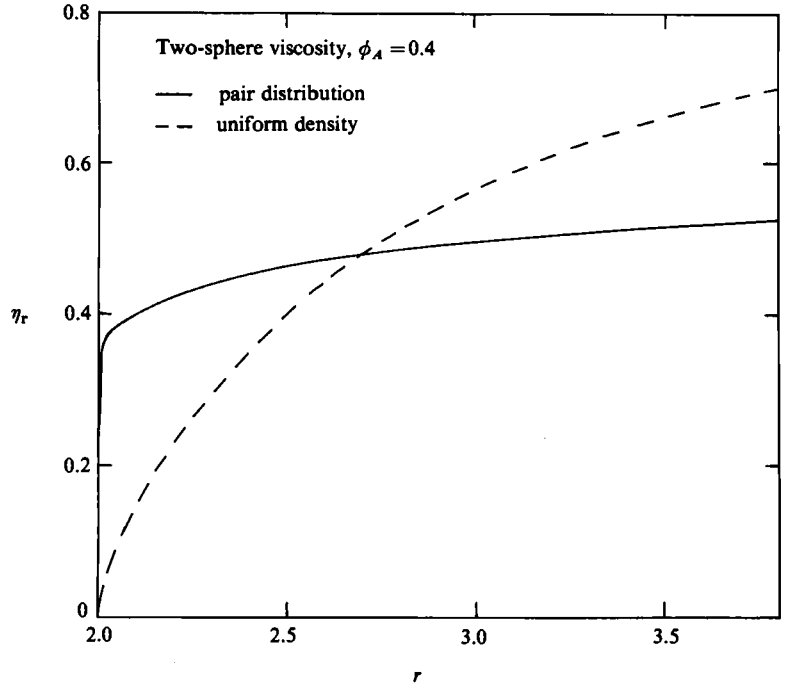

FIGURE 3. The cumulative two-sphere viscosity at $\phi_A = 0.4$ as a function of separation distance r. With a uniform density there is a slow monotonic rise in the cumulative viscosity. With structure, the viscosity rises rapidly in response to the first-nearest-neighbour peak (see figure 5), and then increases more slowly than without structure.

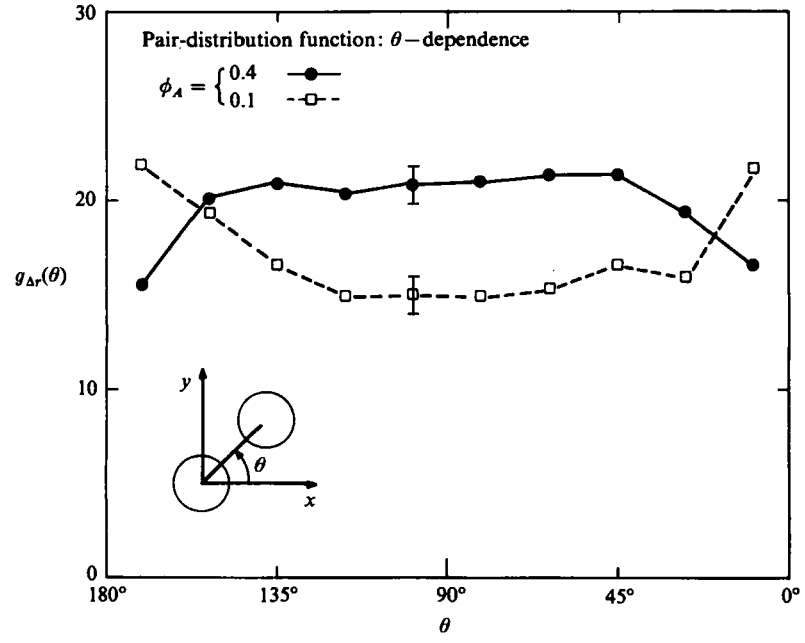

FIGURE 4. The θ-dependence of the pair-distribution function $g_{\Delta r}(\theta)$ in the Δr range $2 \leqslant r \leqslant 2.05$ at two areal fractions $\phi_A = 0.1$ and 0.4. The inset shows the angle θ in relation to the two spheres and the shear flow shown in figure 1. The symmetry of $g_{\Delta r}(\theta)$ about $\theta = 90°$ implies that there are no normal-stress differences with purely hydrodynamic interactions.

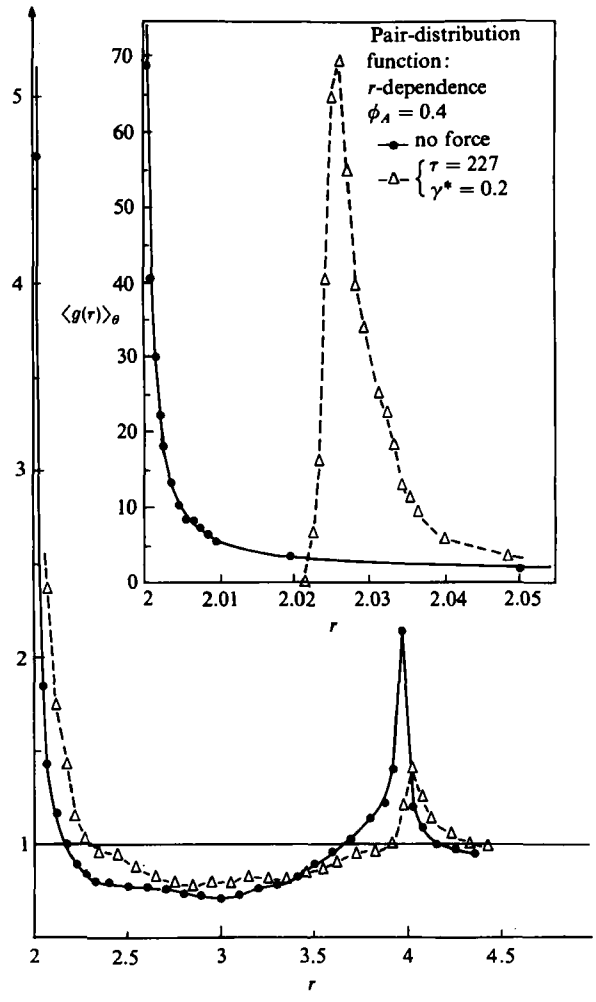

FIGURE 5. The radial dependence of the pair-distribution function $\langle g(r)\rangle_\theta$, which is a simple θ-average, at $\phi_A = 0.4$. The solid curve —●— is the pure hydrodynamic distribution, and the dashed curve —△— is the distribution in the presence of repulsive interparticle forces at $\dot{\gamma}^* = 0.2$ and $\tau = 227$.

the bulk. The form of $\langle g(r)\rangle_\theta$ is quite different from the hard-sphere equilibrium distribution commonly employed in statistical mechanics. Although it is difficult to be precise numerically, rather than reaching a finite value at contact as for hard spheres, $\langle g(r)\rangle_\theta$ appears to be singular (but integrable) as $r \to 2$, reminiscent of the two-sphere distribution found by Batchelor & Green (1972*b*) for extensional flow where $g(r) \sim \xi^{-0.781} (\ln \xi^{-1})^{-0.29}$ as $\xi \to 0$. Also, the width of the first peak, defined as the distance at half-maximum, is very narrow, $O(10^{-3})$.

With the help of figure 5 we can now explain why the two-sphere viscosity with structure is less than without. With structure the cumulative two-sphere viscosity in figure 3 rises rapidly in response to the first-nearest-neighbour peak (recall that the stresslet at contact is finite), but, once the distribution drops below the uniform level at $r = 2.2$, the contribution to the viscosity from this region is less than in the absence of structure, because there are fewer particles; hence the viscosity increases less rapidly with r. By the time the second-nearest-neighbour peak is reached, the

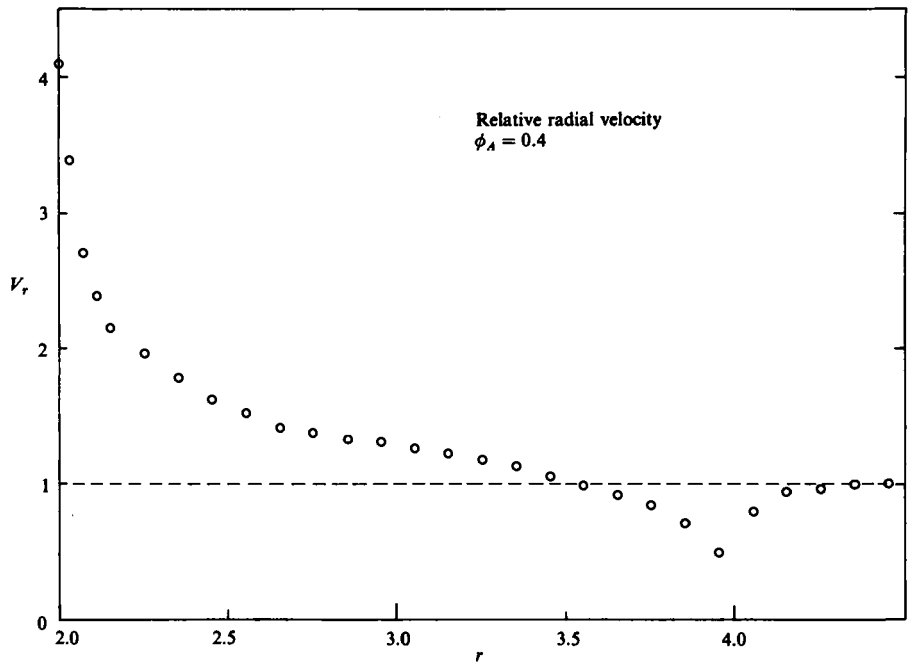

FIGURE 6. The relative radial velocity V_r of two spheres as a function of separation r at an areal fraction of 0.4. V_r is the ratio of the actual relative radial velocity $\Delta U_r^{\alpha\beta}$ of two spheres in suspension to the relative velocity ΔU_r^{B} of two isolated spheres determined by Batchelor & Green (1972*a*). As $r \to 2$, $\xi \to 0$, $\Delta U_r^{\mathrm{B}} \sim -4.077\xi$.

contribution from each particle is so small that this increase in the local density of particles has no effect on the viscosity. The important conclusion to be reached is that the increase in the viscosity with density is not due to the changing microstructure as represented by the pair-distribution function. The microstructure actually results in a lowering of the viscosity.

The increase in the viscosity then must come from the fact that the relative velocities of two particles in suspension differ from their isolated two-sphere values. Perhaps not surprisingly, it is the relative radial velocity $\Delta U_r^{\alpha\beta}$ in (14) that is most important. In figure 6 we present the ratio of the relative radial velocity found in simulation to the two-sphere result of Batchelor & Green (1972*a*) as a function of the centre–centre separation at $\phi_A = 0.4$, i.e. $V_r = \Delta U_r^{\alpha\beta}/\Delta U_r^{\mathrm{B}}$. Recall that the relative radial velocity of Batchelor & Green vanishes as $r \to 2$; $\Delta U_r^{\mathrm{B}} \sim -4.077\xi$ as $\xi \to 0$. V_r also follows the structure closely, decreasing from a maximum of just over 4 to near 1 as the structure relaxes. The motion of two widely separated spheres must of course be uncorrelated, and at large separations V_r approaches unity as $\Delta U_r^{\mathrm{B}} \sim |\boldsymbol{E}\cdot\boldsymbol{r}|$, the independent motion of two spheres.

This large increase in the relative radial velocity, coupled with the high local density at $r \approx 2$, is responsible for the increase in the suspension viscosity above the two-sphere value. The magnitude of V_r at $r = 2$ increases with increasing areal fraction as shown in table 1, and causes the increase in the viscosity with increasing density. It should be noted that, although V_r is approximately 4 at $r = 2$ for $\phi_A = 0.4$, the actual relative radial velocity of two particles vanishes on touching, $\Delta U_r^{\alpha\beta} \sim -16.7\xi$ as $\xi \to 0$; it is only the coefficient of ξ that changes.

The increase in V_r as $r \to 2$ is as if the two spheres find themselves in a shear flow

ϕ_A	$\dot{\gamma}^e$ ($= V_r$ at $r = 2$)	$\dot{\gamma}^e/[1-(\phi_A/\phi_m)^{\frac{1}{2}}]^{-1}$
0.10	1.57 ± 0.10	1.01 ± 0.06
0.25	2.14 ± 0.10	0.932 ± 0.04
0.40	4.02 ± 0.15	1.15 ± 0.04
0.50	5.42 ± 0.20	1.10 ± 0.04

TABLE 1. The effective shear rate $\dot{\gamma}^e$ defined as V_r at $r = 2$ as a function of areal fraction ϕ_A. Note that, although V_r is sharply peaked at $r = 2$, it reaches a constant asymptote for $\xi \leqslant 10^{-3}$. Also shown is the ratio of $\dot{\gamma}^e$ to $[1-(\phi_A/\phi_m)^{\frac{1}{2}}]^{-1}$, indicating that $\dot{\gamma}^e$ scales as $[1-(\phi_A/\phi_m)^{\frac{1}{2}}]^{-1}$ as $\phi_A \to \phi_m$.

with an 'effective' shear rate $\dot{\gamma}^e$, which is larger than the actual shear rate. This increase in $\dot{\gamma}^e$ can be explained by particle clustering. The hydrodynamic lubrication forces cause groups of close particles to act as a single larger particle. A force exerted on one particle at the end of a cluster is 'transmitted', almost as if the particles were in actual contact, to the other end of the cluster via the lubrication forces and the connectivity of the structure. We can imagine a cluster of characteristic length l_c, the cluster size, acting as a rod in the shear flow. In a linear shear flow the stress in the centre of a rod is proportional to its length, and thus two particles finding themselves in the cluster centre experience a shear rate that is $O(l_c - 1)$ times larger than if they were isolated. Particles near the end of a cluster, of course, experience a smaller stress, and hence a lower $\dot{\gamma}^e$. The $\dot{\gamma}^e$ reported in table 1 are averages over all particle pairs and thus over all pairs within a cluster and over all cluster sizes.

In figure 7 a typical (selected at random) particle configuration at $\phi_A = 0.4$ is shown. A group of particles in close contact have been shaded to show the presence of a cluster of 9 particles with characteristic size $l_c = 6$. This cluster is in a region of maximum compression along the 135° line of the shear flow. Both V_r and $\dot{\gamma}^e$ are independent of θ, indicating that, statistically, the cluster is long-lived and rotates *en masse* with the shear flow. The increase in the suspension viscosity with concentration, which results directly from the relative radial velocity, i.e. from $\dot{\gamma}^e$, is the result of the formation of clusters that effectively span large regions of the flow.

Although for all the densities we have simulated we find that the relative radial velocity of two particles vanishes linearly with ξ as the particle surfaces approach one another, the increase in $\dot{\gamma}^e$, the coefficient of ξ, raises the question as to its limiting behaviour at high concentrations. In particular, if $\dot{\gamma}^e$ is proportional to ξ^{-1} as $\phi_A \to \phi_m$, where ϕ_m is some maximum concentration, $\Delta U_r^{\alpha\beta}$ will become finite on touching, and the suspension viscosity will become infinite as discussed in § 1. In a monolayer at high concentrations a simple geometric construction shows that ξ scales as $1-(\phi_A/\phi_m)^{\frac{1}{2}}$ (cf. (3), where the exponent would be $\frac{1}{3}$ for 3 dimensions), and the maximum areal fraction that can still flow is given by a simple cubic arrangement; $\phi_m = \frac{1}{4}\pi = 0.785$. The maximum density $\phi_m = \pi/2\sqrt{3} \approx 0.907$ for hexagonal packing cannot flow in the homogeneous manner considered in this paper.

Shown in table 1 is the ratio of $\dot{\gamma}^e$ to $[1-(\phi_A/\phi_m)^{\frac{1}{2}}]^{-1}$. The simulation results do indeed seem to indicate that $\dot{\gamma}^e$, and hence the viscosity, scale as $[1-(\phi_A/\phi_m)^{\frac{1}{2}}]^{-1}$ as $\phi_A \to \phi_m$. The scaling law leads to the conclusion that the suspension viscosity becomes infinite because of the formation of an infinite cluster, with ϕ_m as a percolation-like threshold. The scaling law for the cluster size is the same as for $\dot{\gamma}^e$, $[1-(\phi_A/\phi_m)^{\frac{1}{2}}]^{-1}$. This cluster formation is the result of the lubrication forces, and thus the same behaviour will occur in three dimensions with a different percolation-like threshold ϕ_m and, using the same simple geometric construction, a $\frac{1}{3}$ in place of $\frac{1}{2}$.

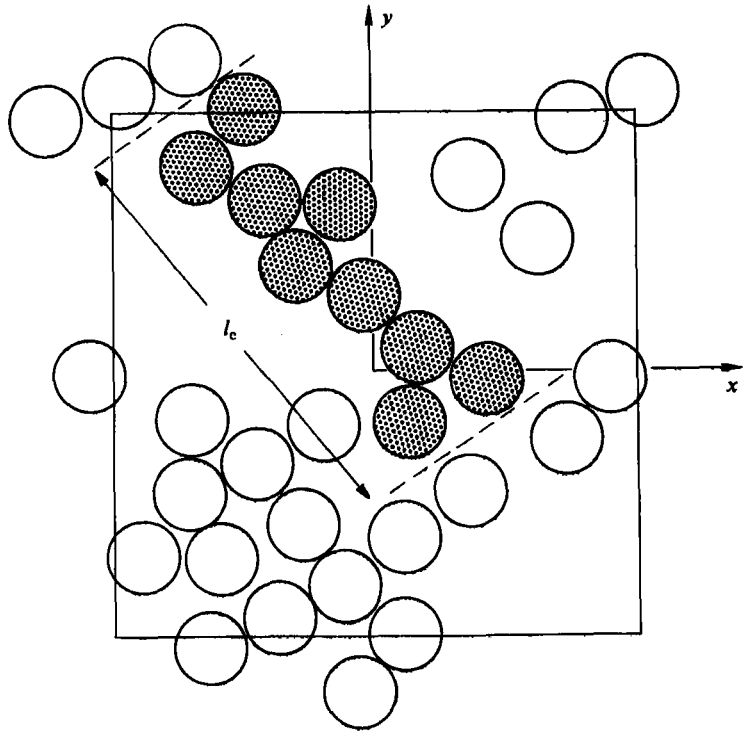

FIGURE 7. A typical particle configuration selected at a random instant in time. The areal fraction is 0.4 and the particles interact purely hydrodynamically. The 9 shaded particles show the presence of a cluster of size $l_c \approx 6$ located in a region of maximum compression along the 135° line of the shear flow. The increase in cluster size with areal fraction is responsible for the increase in the suspension viscosity.

The singular viscosity behaviour is the same as that found by Frankel & Acrivos (1967) from a static lubrication analysis. The origin of the infinite force that is needed in their analysis to push surfaces together at finite velocity comes from the formation of an infinite cluster. Unlike the spatially periodic case, where particles only spend an $O(\xi)$ amount of time at close contact and the viscosity is $O(1)$, the infinite cluster has an $O(1)$ lifetime. Bouillot *et al.* (1982), who conducted sheared monolayer experiments, measured cluster sizes as a function of concentration. Since particles never actually touch one another, it is difficult to give a precise definition of what constitutes a cluster, i.e. how close must two spheres be to belong to the same cluster? Bouillot *et al.* used the limitation of experimental measurement as their definition, giving from their photographic technique a minimum separation of 0.1 radii. Perhaps a better definition would be the half-width of the V_r peak near $r = 2$, or some similar quantity. Nevertheless, their measurements agree remarkably well with the scaling law $l_c \sim [1-(\phi_A/\phi_m)^{\frac{1}{2}}]^{-1}$ (cf. their figure 3). More detailed measurements of suspension microstructure are needed, however, to verify this scaling law.

While the simulation results seem to indicate the formation of an infinite cluster and a singular viscosity, some comments and some caution are in order. The density range we have investigated is limited, and it is possible that a different behaviour will emerge at higher densities. All that can be concluded for certain is that the viscosity increases because of $\dot{\gamma}^e$, and that over the range of densities investigated

$\dot{\gamma}^e$ has a singular scaling law. Once a cluster has grown to the size of the periodic box, its behaviour will be influenced by the periodicity and may not be representative of an infinite suspension.

We have called ϕ_m a percolation-like threshold because of the obvious analogy with percolation phenomena. ϕ_m, however, should not be confused with the classic percolation threshold of, say, a conductivity problem. There is a distinct directionality associated with the shear flow, and the range of interactions is much longer in a suspension. Furthermore, although ϕ_m and the $\frac{1}{2}$ in the scaling law seem to be given accurately by a simple cubic arrangement, it is quite possible that the true percolation threshold lies slightly below $\frac{1}{4}\pi$. Also, the geometric arrangements that lead to the $\frac{1}{2}$ may not be appropriate if the cluster formation has a fractal dimensionality. Finally, it is also possible that $\dot{\gamma}^e$ could scale more strongly than ξ^{-1} with cluster size, resulting in a viscosity that is more singular than that given by (3). Only by simulation at higher densities and with larger systems can these interesting questions be resolved.

From an experimental point of view, the formation of large clusters means that boundary effects will become important. In a typical Couette device one minimizes wall effects by having the gap-to-particle size as large as possible. With the formation of clusters, one must have the gap-to-*cluster* size large in order to minimize wall effects, as the cluster size is now the appropriate microstructural lengthscale. As $\phi \to \phi_m$ the cluster becomes infinite, and wall effects can never be neglected. At high ϕ measured properties are no longer 'material' properties, but functions of the experimental apparatus as well. Finally, since particles spend a large time in very close contact, with separation distances $O(10^{-8})$, surface roughness and non-hydrodynamic forces may become important, if not dominant, at high concentration.

We now turn to a comparison of our simulation viscosities with experiment. Comparison will be made both with the monolayer experiments of Belzons *et al.* (1981) and with three-dimensional suspensions. In order to compare two- and three-dimensional results, the areal and volume fractions will be normalized by the maximum flowing fractions. In two dimensions $\phi_m^{2d} = \frac{1}{4}\pi \approx 0.785$, a simple cubic arrangement. In three dimensions the maximum flow fraction is not known, and we have chosen $\phi_m^{3d} = 0.605$, which corresponds to hexagonal packing perpendicular to the plane of shear, the (x, z)-plane in figure 1, and simple cubic packing in the plane of shear, the (x, y)-plane. This is surely a reasonable value, and other packing arrangements do not give widely different maximum concentrations.

In figure 8 we compare our simulation viscosities (solid circles) with experiment ($\bigcirc$, $\diamond$, $\triangle$) and with the theoretical predictions of Beenakker (1984) ($+$). The symbol size is an indication of the scatter in the experimental data and the statistical uncertainty in the simulations. Let us first examine the monolayer results of Belzons *et al.*, which are the open triangles.

In the experiments of Belzons *et al.* a layer of oil of depth $2a$ was loaded with spheres of radii a and floated on top of water. Above the oil layer was air. This system was placed in a large Couette device, sheared, and the resulting torque measured in the usual fashion. The system is close to our model suspensions, except that in simulation the fluid above and below the plane of particles is the same as in the monolayer. Our simulation viscosities are uniformly larger than the experimental values, although agreement is good at low areal fractions.

There are several possible reasons for these differences. (1) The air and water layers definitely have some effect on the particle interactions and hence the viscosity, but the details of this effect are not known. (2) In the simulation all particles are constrained to lie in the plane of shear, while experimentally only surface tension

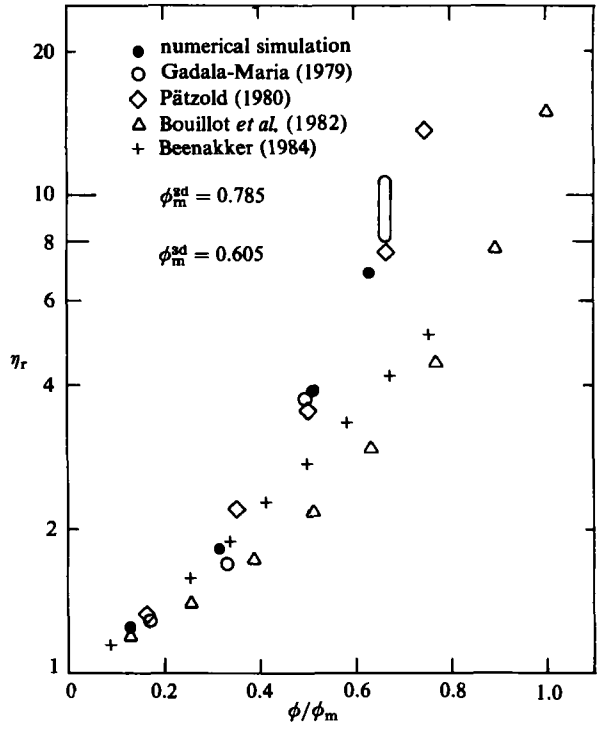

FIGURE 8. Comparison of the simulation viscosities (●) with experiment (○, △) and with the theoretical predictions of Beenakker (1984) (+). All densities have been normalized by the maximum flowing fraction, $\phi_m^{2d} = 0.785$ and $\phi_m^{3d} = 0.605$, to compare 2- and 3-dimensional results. The symbol size is an indication of the experimental error and the statistical uncertainty in the simulations.

keeps the particles in the oil layer. At high concentrations a particle can follow a path of lower resistance by popping up slightly out of the plane of shear. This extra freedom will reduce close contacts and thus lower the viscosity. Finally, (3) it was observed experimentally that above an areal fraction of 0.4 the particles started to form a 'plug', and the shear rate was no longer uniform throughout the gap. At these high concentrations wall effects are evidently important as the cluster size becomes comparable to the gap width. Indeed, Belzons *et al.* performed experiments at $\phi_A = 0.85$, well above the maximum flowing fraction, and noted that the suspension moved as a block with a thin shear layer adjacent to the inner cylinder. This behaviour is radically different from the homogeneous shear flow treated in our simulations. Considering all these factors, the agreement is still quite reasonable (within a factor of 2 or 3), and should be viewed as an indication that the Stokesian-dynamics method contains the essential physics and is capable of quantitative predictions.

The comparison with the three-dimensional experimental results of Gadala-Maria (1979) (○) and Pätzold (1980) (◇) is remarkable. We have selected these data because they are among the most recent and because great care has been taken to minimize non-hydrodynamic effects. Although the agreement is excellent, one should note that the ratio of the normalization densities, ϕ_m^{2d} to ϕ_m^{3d}, acts as an adjustable parameter. Different values of ϕ_m^{3d} will shift the experimental points laterally, but not significantly for reasonable choices of ϕ_m^{3d}. Although the 2-dimensional and 3-dimensional systems

are different and one should not necessarily expect such good agreement, the idea of cluster formation makes this comparison reasonable. If ϵ measures the distance from ϕ_m, $\epsilon = 1-\phi/\phi_m$, then in both 2 and 3 dimensions η_r scales as ϵ^{-1}. What is surprising is that the coefficients are close. We view this agreement as another indication that the approximation of pairwise additivity of forces made in the Stokesian-dynamics method has not lost the proper physics. Indeed, the cluster formation, which is responsible for the increase in the viscosity, results from the lubrication forces and these have been modelled correctly in our method.

Lastly, we turn to a discussion of Beenakker's theoretical predictions, the +s in figure 8. As mentioned in § 1, Beenakker's treatment of the hydrodynamic interactions is in principle exact, although it is not possible to sum completely all interactions. His treatment of dense systems is in the form of a density-fluctuation-correlation expansion about a homogeneous mean state. No calculations of the microstructure are attempted; the Percus–Yevich hard-sphere distribution is used to generate the density fluctuations. Beenakker's predictions are uniformly below the experimental data, but agree well up to volume fractions $\phi \approx 0.25$. The trend at high concentrations is, however, considerably below that of the experiments. While an excellent advancement in suspension theory, Beenakker's predictions apparently fall short for two reasons: (1) the lubrication forces are not completely accounted for because they can only be obtained by summing *all* interactions, and (2) the starting state for the density-fluctuation-correlation expansion does not contain the notion of a percolating cluster.† Both of these are elements we have found to be essential at high concentrations.

3.2. *Interparticle forces*

The addition of non-hydrodynamic forces changes both the suspension microstructure and its rheology. To understand how these changes come about, we have investigated a suspension with one type of interparticle force. In addition to the hydrodynamic forces discussed earlier, particles interact through pairwise repulsive DLVO-type colloidal forces (Vervey & Overbeek 1948; Takamura *et al.* 1981) of the form

$$\boldsymbol{F}^{\alpha\beta} = \boldsymbol{F}_0 \frac{\tau \mathrm{e}^{-\tau\xi}}{1-\mathrm{e}^{-\tau\xi}}. \tag{15}$$

Here $\boldsymbol{F}^{\alpha\beta}$ is, as before, the force on particle α due to particle β, ξ is the separation between particle surfaces, $\tau = \kappa a$, and κ^{-1} is the Debye length. The amplitude $\boldsymbol{F}_0$ acts along the line of centres, is repulsive and is given in magnitude by

$$|\boldsymbol{F}_0| = 2\pi\epsilon\psi^2,$$

where ϵ is the electrical permittivity of the fluid and ψ is the surface potential when $\xi \to \infty$. The form of (15) assumes that the particles move relative to one another at constant surface charge.

The important characteristics of this repulsive force are that it behaves as ξ^{-1} as $\xi \to 0$, just like the lubrication forces, and that it decays to $O(10^{-2}|\boldsymbol{F}_0|\tau)$ when $\xi = O(4.5\tau^{-1})$. $|\boldsymbol{F}_0|$ sets the magnitude of the force and τ sets its range in space. Values for ψ and κ were taken from Takamura *et al.* (1981). For polystyrene latex spheres of 2 μm radius in a 50 % glycerol-in-water mixture containing 10^{-3} M-KCl they report $\psi \approx 4\times10^{-3}$ V and $\kappa^{-1} \approx 88$ Å, giving $\tau \approx 227$. In the simulations reported here the

† Owing to the complexity of Beenakker's analysis, it is difficult to pinpoint the significant approximations, but we feel the abovementioned two are important.

areal fraction and τ were fixed at 0.4 and 227 respectively, and the non-dimensional shear rate $\dot{\gamma}^* = 6\pi\eta a^2\dot{\gamma}/|\boldsymbol{F}_0|$ was varied.

As mentioned in §1, interparticle forces affect the suspension viscosity in two ways: (1) there is the direct 'elastic' contribution to the bulk stress given by (10), and (2) there is an indirect effect through the changing microstructure. They may also create normal-stress differences if the microstructure is not symmetric about $\theta = \frac{1}{2}\pi$ in the plane of shear. In figures 9 and 10 we present the primary normal-stress coefficient Ψ_1 and viscosity η_r over the shear-rate range $10^{-1} < \dot{\gamma}^* \leqslant 10^4$.

The normal-stress differences, of which Ψ_1 is representative, result from the angular structure created by the interparticle forces. As shown in our earlier work (cf. figures 3 and 4 of Bossis & Brady 1984), there is a pronounced angular structure with a maximum at $\theta \approx 135°$ where the shear and repulsive forces balance, and a minimum at $\theta \approx 45°$ where the shear and repulsive forces act together to separate particles. As seen in figure 9 the normal-stress differences increase with increasing concentration and decrease linearly with $\dot{\gamma}^{*-1}$ as $\dot{\gamma}^* \to \infty$. At very low densities, $\phi_A = 0.1$, the normal-stress differences are small, even though there is still a significant angular structure (cf. figure 5 of Bossis & Brady 1984). For spherical particles normal-stress differences are inherently two-body effects and thus $O(\phi^2)$. The linear dependence of Ψ_1 on $\dot{\gamma}^{*-1}$ is in agreement with the experimentally measured normal-stress differences of Gadala-Maria (1979). Neither Gadala-Maria nor we observed a tendency for Ψ_1 to approach a constant as $\dot{\gamma}^* \to 0$, as expected for viscoelastic materials. This is probably due to the fact that a $\dot{\gamma}^* = O(10^{-1})$ is still large. In the limit $\dot{\gamma}^* \to 0$ only the repulsive forces remain, and the suspension should have a regime of elastic response near $\dot{\gamma}^* = 0$. It should be noted, however, that for small $\dot{\gamma}^*$ the Péclet number becomes small and Brownian motion must be considered.

Figure 10 shows the shear-rate dependence of the effective viscosity. The suspension is shear-thickening, but the viscosity calculated using the two-sphere analysis of Batchelor & Green (1972*b*) including both the interparticle-force term $\langle \boldsymbol{S}^{\mathrm{P}} \rangle$ and the microstructure is shear-thinning. There are essentially three effects taking place in the suspension: (1) there is a shear-thinning effect due to the fact that the 'elastic' stresses are proportional to $\dot{\gamma}^{*-1}$ (cf. the last term in (15)); (2) the changing pair-distribution function has some very subtle effects that can be both shear-thickening and shear-thinning; and (3) the formation of particle clusters as $\dot{\gamma}^* \to \infty$ increases the viscosity.

Shown in figure 5 is the radial dependence of the pair distribution function $\langle g(r) \rangle_\theta$ at $\dot{\gamma}^* = 0.2$. Recall that this is a θ-average. Unlike the distribution function without forces, the first-nearest-neighbour peak is sharply peaked at $r \approx 2.027$, where the shear and repulsive forces balance at $\theta \approx 135°$. As the shear rate increases, the first peak increases in height, narrows and is pushed towards $r = 2$. At $\dot{\gamma}^* = 10^4$ the first peak has a height $O(4 \times 10^3)$ and is centred at $r \approx 2 + 3.5 \times 10^{-5}$, i.e. $\xi \approx 3.5 \times 10^{-5}$. The increase in the number of very close neighbours increases the viscosity as explained in §3.1, but, at the same time, the increased region of $\langle g(r) \rangle_\theta < 1$ lowers the viscosity. Since the 'elastic' stresses always (for this particular force that behaves as ξ^{-1}) shear-thin, the two-sphere viscosity indicates that the net result of the changing pair-distribution function is to cause shear thinning.

The shear-thickening behaviour of the simulations comes from the formation of clusters as $\dot{\gamma}^* \to \infty$. The repulsive forces effectively break the connectivity of the clusters, especially on the downstream side $\theta < \frac{1}{2}\pi$, and diminish their ability to transmit stress. At $\dot{\gamma}^* = 0.2$, the $\dot{\gamma}^{\mathrm{e}}$ at the location of the first peak was only approximately 2, as compared with 4 in the absence of forces. Snapshots of the

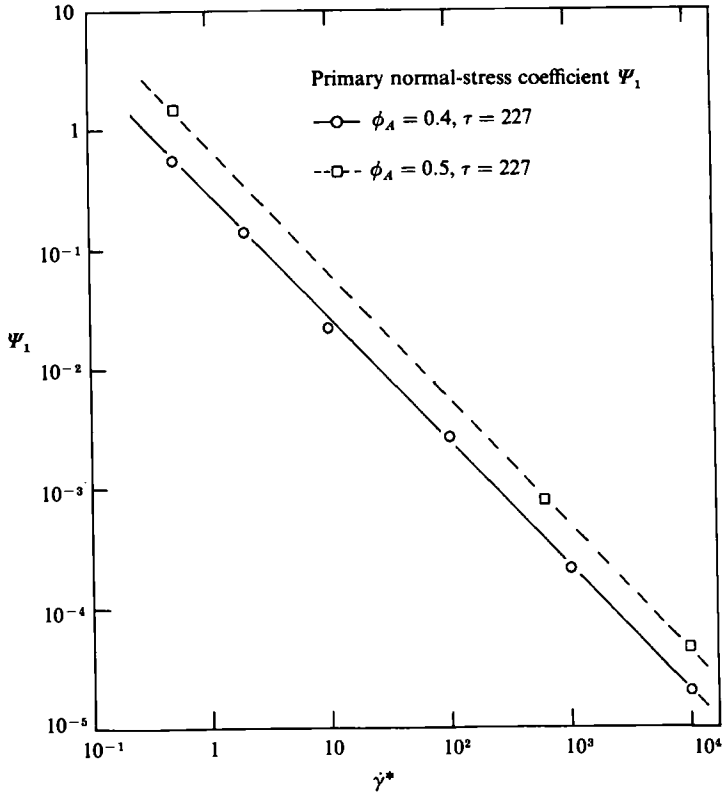

FIGURE 9. The primary normal-stress coefficient Ψ_1 as a function of $\dot{\gamma}^*$ for two areal fractions $\phi_A = 0.4$ and 0.5. The range of the interparticle force was kept constant, $\tau = 227$. Ψ_1 decreases linearly with $\dot{\gamma}^{*-1}$.

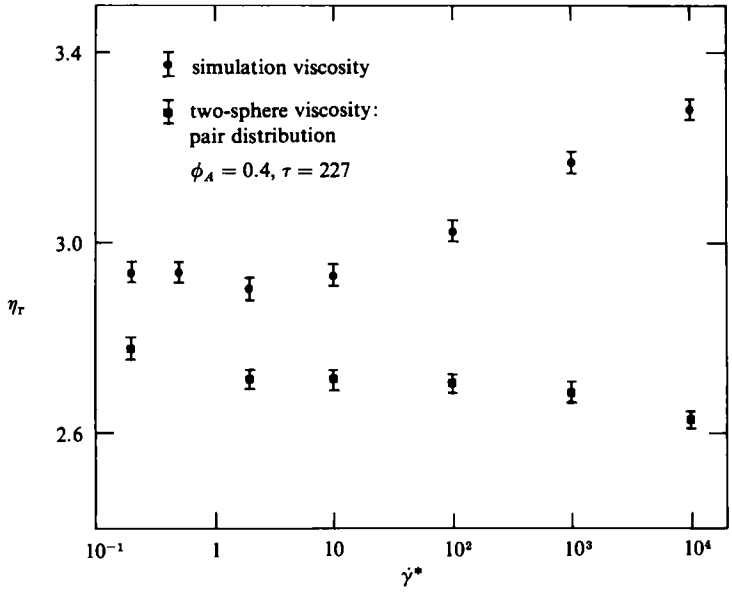

FIGURE 10. The shear-rate dependence of the suspension viscosity at $\phi_A = 0.4$. The simulations show a shear-thickening behaviour due to the increased formation of clusters as $\dot{\gamma}^* \to \infty$. The two-sphere viscosities show a shear-thinning behaviour because they contain no information on cluster formation.

particle distribution, as in figure 7, with forces (cf. figure 12 of Bossis & Brady 1984) show a much more homogeneous and open structure with smaller cluster sizes. Again clustering seems to play a very important role in the suspension viscosity.

The shear-rate dependence of the effective viscosity and the arguments given here to explain it are applicable for this particular interparticle force. It is not known whether other forces will give rise to the same qualitative behaviour, or will be fundamentally different. The subtle interplay of the microstructure, the interparticle forces, and the cluster formation makes general statements difficult. We hope that, as more information becomes available for other types of forces, a clearer picture will emerge.

4. Conclusions

We have shown how the general method of Stokesian dynamics can be used to compute macroscopic rheological properties of suspensions. For suspensions in which particles interact through purely hydrodynamic forces, it was shown that the increase in the suspension viscosity with increasing volume fraction can be interpreted as due to the formation of particle clusters. Microstructural effects embodied in the concentration dependence of the pair-distribution function were shown to result in a suspension viscosity that was lower than in the absence of structure. Over the concentration range investigated in the monolayer simulations, the cluster size l_c was seen to scale as $l_c \sim [1-(\phi_A/\phi_m)^{\frac{1}{2}}]^{-1}$, where $\phi_m = \frac{1}{4}\pi$. This scaling law predicts the formation of an infinite cluster at the percolation-like threshold ϕ_m, and predicts that the suspension viscosity becomes singular with the same scaling law. Three-dimensional suspensions are expected to have a similar scaling law, with a different percolation-like threshold. The cluster formation is a direct result of the hydrodynamic lubrication forces that keep particle surfaces from touching. The predicted suspension viscosities were shown to be in good agreement with experiment, indicating that the approximation of pairwise additivity of forces in the resistance matrix contains the essential physics.

These stimulations are intended to model the behaviour of a homogeneously sheared suspension in regions far removed from any boundaries. As a result, there is a maximum volume fraction ϕ_m that can flow in a homogeneous manner. It is possible to shear suspensions at concentrations above ϕ_m, but then the average motion will not correspond to the homogeneous shear flow considered here. At these high densities it is likely that small regions of the suspension, perhaps adjacent to the boundaries, will shear rapidly, leaving the rest of the suspension immobile. Indeed, the idea of the formation of an infinite cluster as $\phi \rightarrow \phi_m$ implies that boundary effects will dominate at the percolation-like threshold. Also, at high densities particle surfaces become arbitrarily close to one another, and non-hydrodynamic forces and/or surface roughness will ultimately play a very important role in suspension behaviour. These observations may explain why the scatter in the experimental data is pronounced at high volume fractions, and why normal-stress differences and shear-rate-dependent behaviour are often observed. Normal-stress differences and rate-dependent viscosities cannot occur in a purely hydrodynamically interacting suspension.

The DLVO-type repulsive interparticle forces investigated here were seen to be effective at reducing cluster formation and thus lowering the suspension viscosity. As a result, the suspension shear-thickens as the hydrodynamic forces gain importance and reform the clusters. The anisotropic local structure caused by the interparticle

forces gives rise to normal-stress differences. It is difficult, however, to make general statements about the precise role of interparticle forces on suspension rheology, because of the subtle interplay of the forces, the changing microstructure and the cluster formation. Further simulation studies with different types of forces are needed to clarify this area.

We hope we have shown that the Stokesian-dynamics method is capable of quantitative predictions of macroscopic behaviour, as well as providing a thorough understanding of how the fundamental mechanisms operating on the microscale affect this behaviour. The generality of the method allows a variety of problems to be studied, and it can readily be extended to include boundary effects and Brownian motion, opening up an even broader class of suspension problems.

This work was supported in part by a grant from the Centre National de la Recherche Scientifique under the ATP programme in macroscopic random materials and by a grant from Monsanto Company. Computer time was kindly provided by the Centre de Calcul Vectoriel pour la Recherche on the Cray at Ecole Polytechnique. Finally, we thank Drs D. J. Jeffrey and S. Kim for providing us with their calculations of the two-sphere resistance functions.

REFERENCES

ADLER, P. M., ZUZOVSKY, M. & BRENNER, H. 1985 *Intl J. Multiphase Flow* (to appear).

ARP, P. A. & MASON, S. G. 1977 *J. Coll. Interface Sci.* **61**, 21.

BAGNOLD, R. A. 1954 *Proc. R. Soc. Lond.* A **225**, 49.

BATCHELOR, G. K. 1970 *J. Fluid Mech.* **41**, 545.

BATCHELOR, G. K. 1974 *Ann. Rev. Fluid Mech.* **6**, 227.

BATCHELOR, G. K. 1977 *J. Fluid Mech.* **83**, 97.

BATCHELOR, G. K. & GREEN, J. T. 1972*a* *J. Fluid Mech.* **56**, 375.

BATCHELOR, G. K. & GREEN, J. T. 1972*b* *J. Fluid Mech.* **56**, 401.

BEENAKKER, C. W. J. 1984 *Physica* A **128**, 44.

BEENAKKER, C. W. J. & MAZUR, P. 1983 *Physica* A **120**, 338.

BELZONS, M., BLANC, R., BOUILLOT, J. L. & CAMOIN, C. 1981 *C. R. Acad. Sci. Paris* **292**, 939.

BOSSIS, G. & BRADY, J. F. 1984 *J. Chem Phys.* **80**, 5141.

BOUILLOT, J. L., CAMOIN, C., BELZONS, M., BLANC, R. & GUYON, E. 1982 *Adv. Coll. Interface Sci.* **17**, 299.

BRENNER, H. 1974 *Intl J. Multiphase Flow* **1**, 195.

EINSTEIN, A. 1906 *Annalen Phys.* **19**, 298 (and **34**, 591).

EVANS, D. J. 1979 *Mol. Phys.* **37**, 1745.

FRANKEL, N. A. & ACRIVOS, A. 1967 *Chem. Engng Sci.* **22**, 847.

GADALA-MARIA, F. A. 1979 Ph.D. Thesis, Stanford University.

GADALA-MARIA, F. A. & ACRIVOS, A. 1980 *J. Rheol.* **24**, 799.

HOFFMAN, R. L. 1972 *Trans. Soc. Rheol.* **16**, 155.

HUSBAND, D. M. & GADALA-MARIA, F. A. 1984 *Proc. 9th Intl Congr. Rheology, Acapulco, Mexico.*

JEFFREY, D. J. & ACRIVOS, A. 1976 *AIChE J.* **22**, 417.

JEFFREY, D. J. & ONISHI, Y. 1984 *J. Fluid Mech.* **139**, 261.

KIM, S. & MIFFLIN, R. T. 1985 *Phys. Fluids* (to appear).

KRIEGER, I. M. 1972 *Adv. Coll. Interface Sci.* **3**, 111.

MAZUR, P. & VAN SAARLOOS, W. 1982 *Physica* A **115**, 21.

NUNAN, K. C. & KELLER, J. B. 1984 *J. Fluid Mech.* **142**, 269.

O'Brien, R. W. 1979 *J. Fluid Mech.* **19**, 17.
Pätzold, R. 1980 *Rheol. Acta* **19**, 322.
Peterson, J. M. & Fixman, M. 1963 *J. Chem. Phys.* **39**, 2516.
Russel, W. B. 1978 *J. Fluid Mech.* **85**, 673.
Russel, W. B. 1980 *J. Rheol.* **24**, 287.
Vervey, E. G. & Overbeek, J. T. G. 1948 *Theory of the Stability of Lyophobic Colloids*. Elsevier.